

Rotational Stabilization of Resistive Wall Mode on JT-60U^{*}

Go MATSUNAGA, Manabu TAKECHI, Nobuyuki AIBA, Genichi KURITA,
Yoshiteru SAKAMOTO, Yoshihiko KOIDE, Akihiko ISAYAMA, Takahiro SUZUKI,
Takaaki FUJITA, Naoyuki OYAMA, Takahisa OZEKI, Yutaka KAMADA and JT-60 Team

Japan Atomic Energy Agency, Naka 311-0193, Japan

(Received 24 July 2009 / Accepted 14 August 2009)

We have carried out experiments to clarify the stabilizing effect of a plasma rotation on the resistive wall mode (RWM) that could limit the achievable- β_N in high- β_N plasmas above the no-wall ideal β_N -limit. On JT-60U plasma rotations are controlled using neutral beams with varying combinations of net torque input while keeping β_N constant. The RWM is destabilized as the plasma rotation is being reduced. Detailed measurements of the mode structure revealed that the RWM has a global structure that rotates with the order of the resistive wall time. In these experiments, it is found that the critical toroidal rotation speed for the RWM stabilization is less than 1% of the Alfvén speed. Moreover, the critical rotation does not strongly depend on β_N . The results suggest that high- β_N operation up to the ideal wall β_N -limit could be possible by suppressing the RWM with a slow plasma rotation in fusion reactors.

© 2009 The Japan Society of Plasma Science and Nuclear Fusion Research

Keywords: resistive wall mode, plasma rotation, JT-60U

DOI: 10.1585/pfr.4.051

1. Introduction

For a future fusion reactor, a steady-state high- β plasma is necessary for it to be economical because the high- β means the high fusion output P_{fus} , which is defined as [1] $P_{\text{fus}} \propto \langle p \rangle^2 \propto \beta_N^2 I_p^2 B_t^2$; where β_N is the plasma pressure normalized by the device parameters of I_p and B_t ; $\beta_N = \beta_t / (I_p / a B_t) \propto \langle p \rangle / (I_p B_t)$. Here, $\langle p \rangle$, β_t , I_p , B_t and a are the volume-averaged plasma pressure, toroidal- β , plasma current, toroidal magnetic field and plasma minor radius, respectively. From the definition of β_N operation in the high- β_N region means high fusion output even with a compact device, that is, the device could be said to be economically efficient. However, the achievable- β_N is limited by ideal MHD instabilities. In such high- β_N plasmas ideal kink-ballooning modes that are driven by both the pressure gradient $\nabla p(r)$ and the plasma current $j(r)$ can limit the achievable- β_N . The ideal MHD theory provides for two limits that are determined by the boundary conditions in the vacuum region surrounded the plasma. The lower limit is the no-wall ideal β -limit (β_N^{free}) that corresponds to the case with a free boundary. The upper limit is the ideal-wall ideal β -limit (β_N^{ideal}) that corresponds to the case with the conducting wall close to the plasma, and the conducting wall has perfect conductivity. In general β_N^{ideal} is larger than β_N^{free} , and hence the ideal-wall can improve the MHD stability. Namely, the region between β_N^{free} and β_N^{ideal} becomes available with an ideal-wall, which can be called the “wall-stabilized high- β_N region.” Meanwhile, because on real-

istic devices the conducting wall has finite resistivity the stabilizing effect is lost due to the wall resistivity [2]. This results in additional instability originating from the wall resistivity, that is, the resistive wall mode (RWM). The RWM is destabilized in the region $\beta_N^{\text{free}} \leq \beta_N \leq \beta_N^{\text{ideal}}$ with a characteristic growth time that corresponds to the skin time of the resistive wall τ_w (resistive wall time). Namely, the growth rate and the mode rotation frequency slow down to the order of τ_w^{-1} . The RWM is predicted to have a global eigen-function similar to that of the ideal mode. The fact that the RWM could limit achievable- β_N in realistic devices makes RWM stabilization a critical issue in achieving steady-state high- β_N operations in ITER and fusion reactors.

Bondeson and Ward predicted that the plasma rotation could stabilize the RWM [3]. In their numerical results the plasma dissipation could couple with the RWM stability via the plasma rotation, and the rotation larger than several percent of the Alfvén speed is required for the RWM stabilization. Several models have been proposed for the rotational stabilization of the RWM [4–7]. If the plasma rotation is to be effective in stabilizing the RWM the required plasma rotation, hereafter referred to as the critical rotation, should be quantitatively validated and experimentally identified because the plasma rotation in ITER and fusion reactors is predicted to be less than 1% of the Alfvén speed [8].

For this reason we have carried out the high- β_N experiments on JT-60U in order to investigate the critical rotation required for the RWM stabilization [11, 12]. Previously, the RWMs were observed in the reversed shear plas-

author's e-mail: matsunaga.go@jaea.go.jp

^{*} This article is based on the invited talk at the 24th JSPF Annual Meeting (2007, Himeji).

mas where β_N^{free} was lower than that in the positive shear plasmas on JT-60U [9]. The resistive wall location effect has also been investigated in the ohmic discharges where the current-driven RWMs are destabilized by decreasing the surface- q below a low integer value [10]. In studying the plasma rotation effect JT-60U has the advantage that the plasma toroidal rotation can be widely controlled using neutral beams (NBs) with varying combination of net torque input. The NBs in JT-60U are composed of co- and counter-tangential and perpendicular injections (See Sec. 2.1). Utilizing the NB system the plasma rotation was changed at a constant β_N in order to evaluate the plasma rotation effect only. Hereafter plasma rotation will be used to denote ‘‘toroidal’’ plasma rotation. This paper provides detailed results of high- β_N experiments that focused on the rotational stabilization of RWM.

2. High- β_N Experiments on JT-60U

2.1 Neutral beam injection system

In order to investigate the critical rotation needed for RWM stabilization the plasma rotation was controlled using neutral beam (NB) injections in JT-60U. As shown in Fig. 1, the JT-60U has various types of NBs [13, 14]. There are 11 positive ion based NBs (P-NBs) with an energy of ~ 85 keV. The P-NBs consist of 4 tangential (TANG-NBs) and 7 perpendicular NBs (PERP-NBs). The TANG-NBs contain 2 co-tangential (in the direction of I_p) and 2 counter-tangential (in the opposite direction of I_p) injections. The power of all the P-NBs is ~ 2 MW. In addition, there are 2 negative ion based NBs (N-NBs) with an energy of ~ 350 keV. Note that the momentum input from the

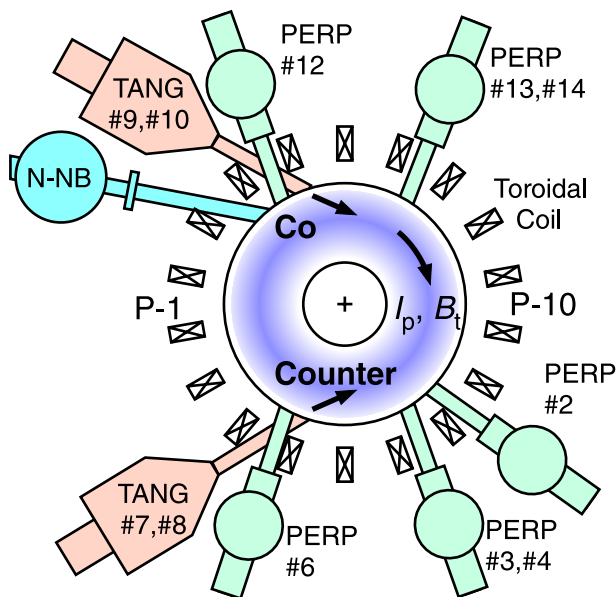


Fig. 1 Top view of the JT-60U torus with NB heating system. PERP and TANG stand for perpendicular and tangential-NBs; N-NB is negative ion based NB.

N-NBs is less than that from the P-NBs because the N-NB beam current is less instead of the high beam energy. These NBs enables both the direction and profile of a plasma rotation to be controlled while keeping β_N by stored energy feedback control.

2.2 Ferritic steel tiles and resistive wall

Before the 2006 experimental campaign, ferritic steel tiles were installed inside the JT-60U vacuum vessel to reduce a toroidal magnetic field ripple that could enhance fast ion ripple loss [15]. For example, the toroidal magnetic field ripple can be reduced from 1.5% to 1.0% at $B_t = 1.6$ T. That reduction improves the absorbed NB power by about 35% with large volume plasmas close to the wall. High- β_N experiments can take place with the plasma close to the wall for wall stabilization with sufficient heating power. Figure 2 gives the poloidal cross section of JT-60U with a plasma and the ferritic steel tiles. The ferritic steel tiles cover the inside of the outboard vacuum vessel where the toroidal ripple is large. In the experiments the plasma was moved close to the outer wall by up to $d/a \approx 1.2$, where d is the wall radius. As mentioned above, a RWM is characterized by the resistive wall time τ_w defined as $\tau_w = \mu_0 d \delta / \eta_w$, where η_w and δ are the wall resistivity and thickness of the resistive wall. The JT-60U vacuum vessel consists of double layers of Inconel 625 whose thickness is 6.1 mm [16]. The resistivity of Inconel is about $1 \times 10^{-6} \Omega\text{m}$, which corresponds to a resistive wall time of $\tau_w \sim 10$ ms. The eddy current on the ferritic steel tiles is thought to be negligible compared with

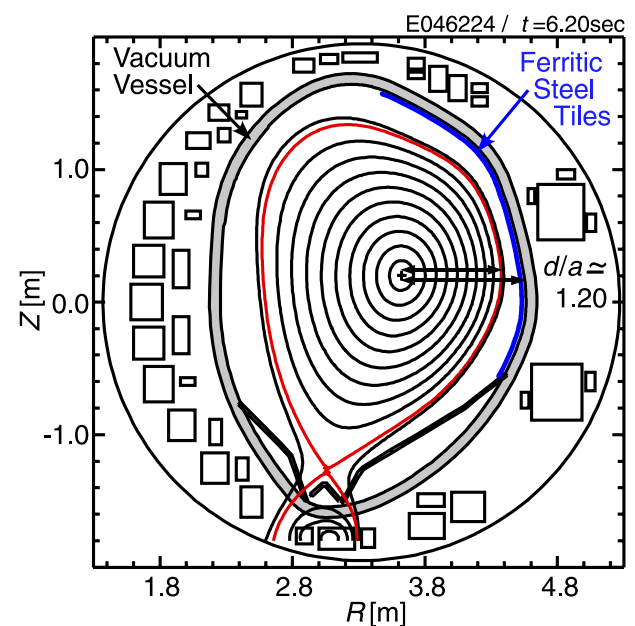


Fig. 2 Poloidal cross section of JT-60U with a plasma and the ferritic steel tiles. The ferritic steel tiles cover the inside of the outboard vacuum vessel. The red line indicates the separatrix.

Inconel vessel because the clearance between the tiles is about 1 cm and each tile has several 2 mm slits to avoid any large eddy currents, and hence with regard to low- n MHD stability it is reasonable to expect that the Inconel vessel only determines the wall effect.

2.3 Experimental results

For the purpose of identifying of the critical rotation needed for RWM stabilization high- β_N experiments were carried out with the plasma close to the outer wall at $d/a \approx 1.2$. As mentioned above, since the ferritic steel tiles improve the NB absorption power, it is possible to access the high- β_N region above β_N^{free} where the wall stabilization is expected. Figure 3 gives the waveforms of a high- β_N discharge where I_p and B_t were 0.9 MA and 1.57 T, respectively. In this discharge, in order to access the high- β_N above β_N^{free} , sufficient momentum input from the TANG-NBs was used to rotate the plasma. The plasma rotations measured using charge exchange recombination

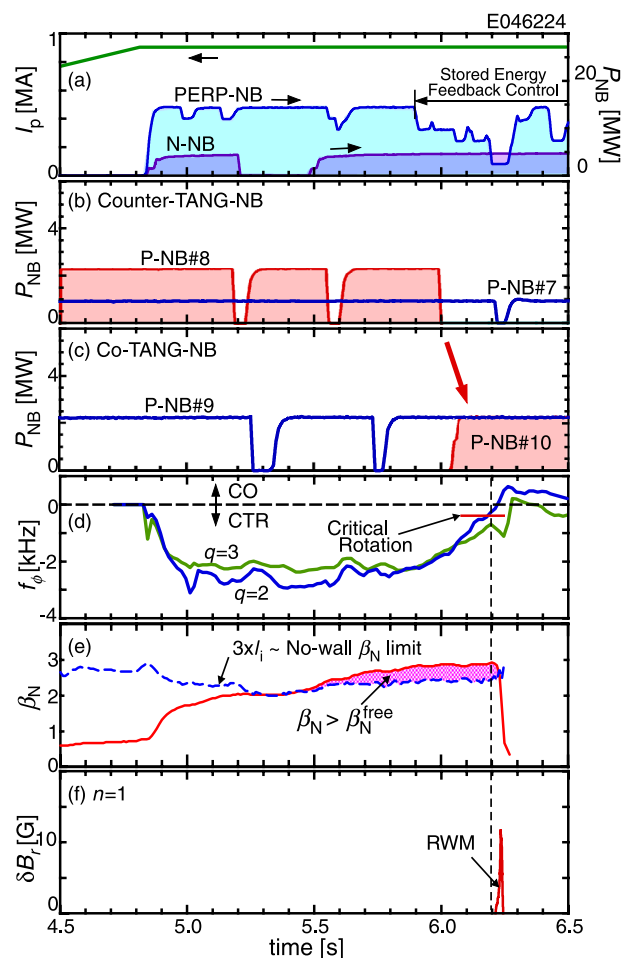


Fig. 3 Waveforms of high- β_N experiment: (a) Plasma current, PERP-NB and N-NB injection power, (b) counter- and (c) co-TANG-NB power, (d) plasma rotation frequency at $q = 2$ and 3 , (e) β_N with $3 I_i \sim \beta_N^{\text{free}}$, (f) $n = 1$ integrated magnetic perturbation.

spectroscopy (CXRS) [17], described here as the angular frequency f_ϕ , were larger than 2 kHz at both the $q = 2$ and $q = 3$ surfaces (Fig. 3 (d)). Continuous NB injection was used to achieve β_N reaching about 2.8 (Fig. 3 (e)). At $t = 6.0$ s one of the counter-NBs was switched to co-NB in order to change only the plasma rotation but not β_N (Figs. 3 (b) and (c)). In addition, in order to keep β_N constant, a stored energy feedback control, which is used to control a number of the PERP-NBs, was applied after $t = 5.9$ s. The plasma rotation then slowly decelerated, and finally a strong β -collapse occurred at $t = 6.23$ s (Fig. 3 (e)). Before the NB switching took place at $t = 6.0$ s, the plasma rotation already began to decelerate. The deceleration is due to the reduced number of PERP-NBs by the stored energy feedback control because the PERP-NBs can drive a contour plasma rotation due to fast ion ripple loss. Ideal MHD stability analysis using MARG2D [18] revealed β_N^{free} to be estimated to be 2.3, that is, $\sim 3 I_i$ [19]. The achieved- $\beta_N \approx 2.8$ exceeded β_N^{free} (Fig. 3 (e)). High- β_N above β_N^{free} was therefore achieved for the time duration of 0.5 s. At $t = 6.21$ s the $n = 1$ instability was growing (Fig. 3 (f)). That instability then finally induced a strong β -collapse.

Figure 4 shows enlarged waveforms in Fig. 3. Just be-

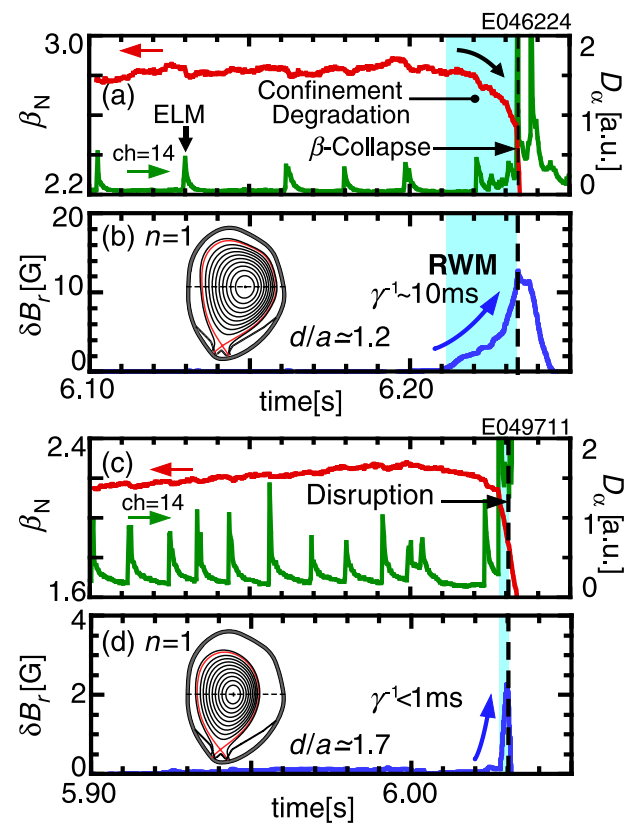


Fig. 4 Expanded waveforms of high- β_N (Fig. 3) and high- β_p discharges just before collapse (disruption): (a) time evolution of β_N and D_α emission, (b) $n = 1$ integrated magnetic perturbation with the poloidal cross section. cf. (c) and (d) give the high- β_p discharge with $d/a \approx 1.7$.

fore the β -collapse an $n = 1$ magnetic perturbation was gradually growing. The growth time of the instability was about 10 ms, which is comparable with the resistive wall time τ_w of JT-60U. During that growth phase the confinement degraded with the same time scale as the instability shown in Fig. 4 (a). Since this instability directly affects the energy confinement it suggests that the instability has a global mode structure. The results indicate that the observed instability is an $n = 1$ RWM. For the sake of comparison, the instability observed in the high poloidal- β (β_p) discharge with $I_p/B_t = 1.5 \text{ MA}/3.57 \text{ T}$ is provided in Figs. 4 (c) and (d). The time ranges with both the plots is 150 ms. Note that a high- β_p discharge is associated with a large internal transport barrier (ITB), and thus a fairly steep pressure gradient exists. In this discharge the plasma was positioned far from the wall with $d/a \approx 1.7$. The discharge was terminated by a disruption that occurred due to an $n = 1$ instability. The growth time of the observed instability was less than 1 ms, which is much shorter than the RWM growth time. It is considered that wall stabilization with $d/a \approx 1.7$ is less effective than with $d/a \approx 1.2$. The instability is thought to be an ideal kink-ballooning mode that becomes unstable as β_N reaches β_N^{free} [20]. However, it is difficult to clearly identify the instability with a large plasma-wall separation because a RWM root continuously connects to the ideal kink-ballooning mode [6].

In the β_N constant phase, ion temperature T_i around the $q = 2$ and $q = 3$ surfaces basically remained un-

changed within an accuracy of $|\Delta T_i/T_i| < 5\%$. Internal inductance l_i slightly increased with $\Delta l_i/l_i \leq 5\%$, which is due to $j(r)$ penetration. These measurements indicate that $\nabla p(r)$ and $j(r)$ basically remained unchanged. It is considered therefore that the RWM became unstable due to the deceleration of the plasma rotation only. As shown in Fig. 4, edge localized modes (ELMs) were continuously observed. While the RWM was growing a final ELM was observed at $t = 6.22 \text{ s}$ without any change in ELM frequency. This then means that the RWM did not seem to have affected the pedestal structure at first. Namely, the RWM began to grow from the core region, thus suggesting the eigen-function to be a large structure inside the plasma.

2.4 Mode structure of RWM

Figures 5 (a) and (b) give the contour plots of the perturbed magnetic field with the high- β_N discharge where the RWM was observed. These were measured using the toroidally-distributed eight saddle loops and poloidally-distributed magnetic probes. The upper plots provide the toroidal distribution of the radial magnetic components δB_r . The lower plots provide the poloidal distribution of the poloidal magnetic components δB_θ . Both signals are integrated, and the toroidal axisymmetric component ($n = 0$) is removed from the upper one.

As seen in Fig. 5 (a) the RWM has a clear $n = 1$ toroidal mode structure. Meanwhile, Fig. 5 (b) reveals that the poloidal structure is not uniform. Namely, the ampli-

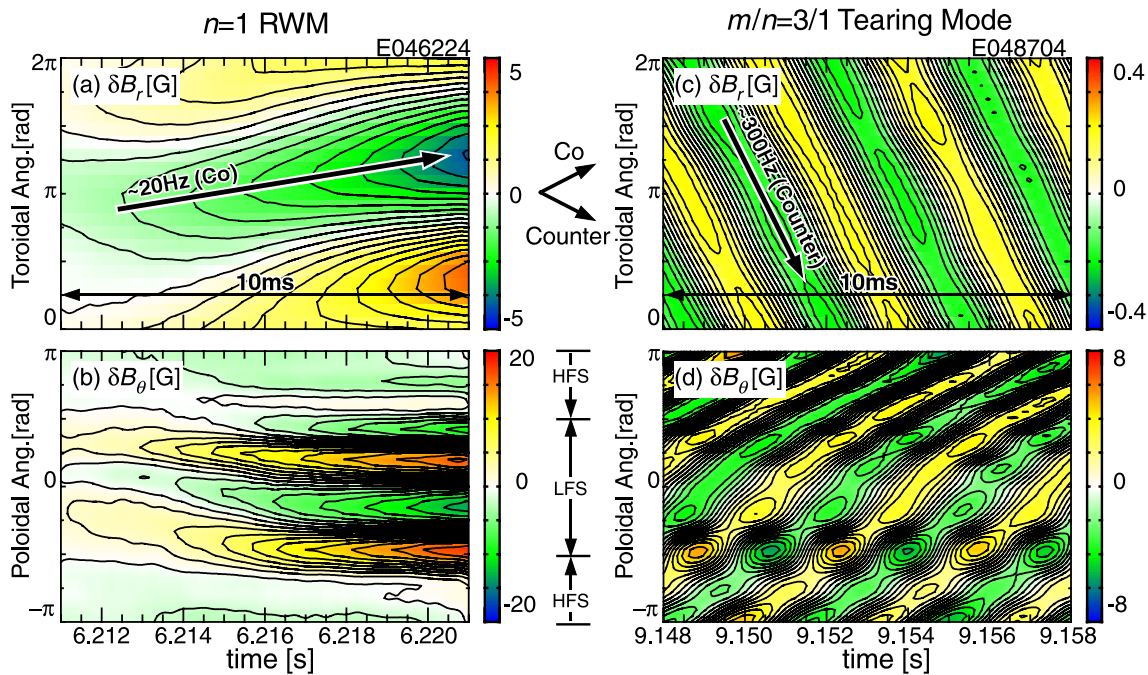


Fig. 5 Comparison of poloidal and toroidal mode structures between $n = 1$ RWM (left) and $m/n = 3/1$ tearing mode (right). Upper plots give the toroidal distributions of perturbed radial magnetic fields δB_r ; lower plots give the poloidal distribution of perturbed poloidal magnetic fields δB_θ . Arrows indicates the direction of the mode rotation. Toroidal angle is defined as the same direction as I_p ; poloidal angle is defined from the midplane at the LFS.

tude at the low field side (LFS: bad curvature) is larger than that at the high field side (HFS: good curvature). Here, the poloidal angle is defined from the midplane at the LFS; the divertor region corresponds to around $-\pi/2$. In Fig. 5 (b), although the poloidal structure seems to have two periods ($m = 2$), the wave length (angle) is not π , and is rather shorter. The dominant poloidal mode number is therefore considered to be $m \geq 3$, and the poloidally non-uniform structure is attributed to the multi poloidal components. This is consistent with the result calculated using MARG2D (See Sec. 2.5). In addition, the RWM was slowly rotating in the co-direction with a mode frequency of ~ 20 Hz. Since the RWM is a wall-trapped mode, a frequency of zero could be predicted if there was no plasma rotation. With a plasma rotation, the RWM is theoretically predicted to have a slow rotation comparable to an order of τ_w^{-1} [3]. Actually, the observed RWM rotated in the co-direction to I_p . The direction was thought to be followed by the direction of the plasma rotation at the $q = 2$ surface. For comparison, the magnetic structures of an $m/n = 3/1$ tearing mode observed in the ohmic discharge are provided on the right-hand side of Fig. 5. In this discharge the $m/n = 3/1$ tearing mode was destabilized only by the plasma current. Since the tearing mode was composed of a single poloidal component the poloidal structure is almost uniform. The mode frequency was about 300 Hz in the counter-direction of I_p . In this discharge, since no NB was injected, the mode frequency was considered to be followed by a spontaneous plasma rotation at the $q = 3$ surface that was determined by the transport.

Figure 6 gives the time evolution of the ion temperature T_i profiles during the growth of the RWM. As the

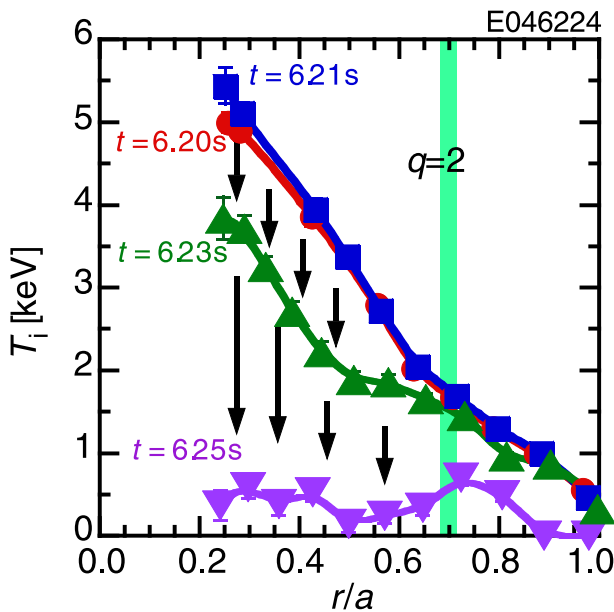


Fig. 6 Time evolution of ion temperature profiles during $n = 1$ RWM growth measured using CXRS.

RWM grew, T_i inside the $q = 2$ surface was gradually dropping, and finally the T_i profile globally lost. This then means that the RWM has a radially extended eigenfunction that is also consistent with the MARG2D results (See Sec. 2.5).

2.5 MHD stability analysis

MARG2D code [18], which is the linear MHD stability analysis code, was used to estimate the MHD stability with and without a conducting wall near the plasma. Note that MARG2D is based on ideal MHD analysis, not including the effect of the resistive wall and the plasma rotation. Figure 7 (a) provides a stability diagram of critical- β_N versus the wall location d/a . Here, $d/a = \infty$ corresponds to the case of no-wall. Decreasing d/a improves the ideal-wall limit, thus, expanding the region between β_N^{free} and β_N^{ideal} . In the region $\beta_N^{\text{free}} \leq \beta_N \leq \beta_N^{\text{ideal}}$ the ideal kink-ballooning mode is stabilized by an ideal-wall, and thus is a wall-

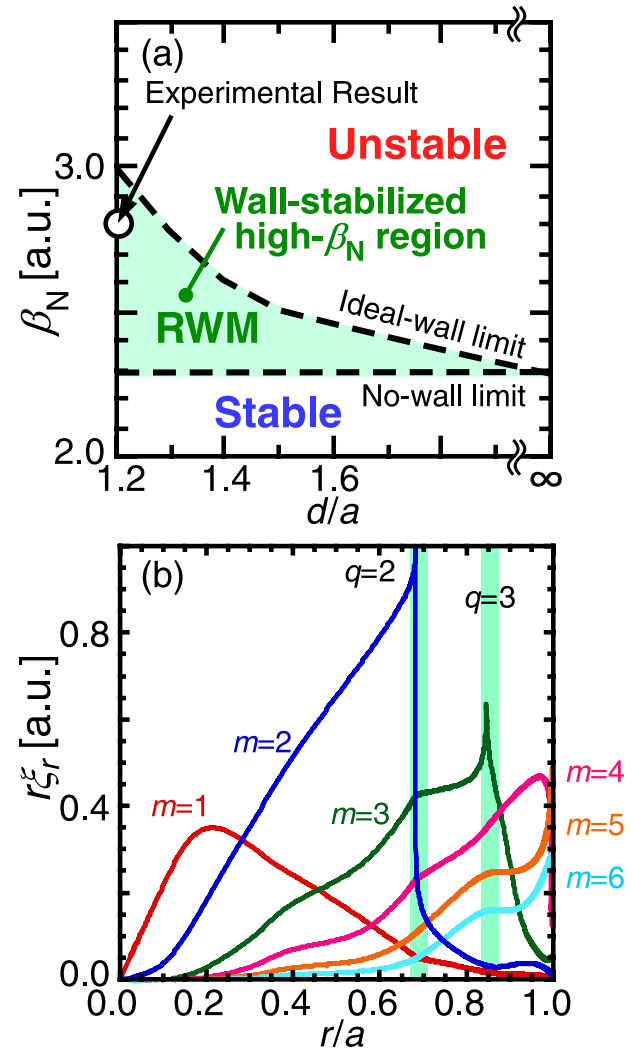


Fig. 7 MARG2D results: (a) Stability diagram of β_N vs wall location d/a , (b) eigen-function of ideal kink-ballooning mode with an ideal-wall.

stabilized high- β_N region. The open circle in Fig. 7 (a) describes the corresponding point in this experiment where the RWM was observed. In the experiment the plasma was stable with an ideal-wall but unstable without a wall. As mentioned above, since RWM was predicted to be unstable in the region $\beta_N^{\text{free}} \leq \beta_N \leq \beta_N^{\text{ideal}}$, that observation is consistent with the prediction. The eigen-function of the ideal mode with an ideal-wall is provided in Fig. 7 (b) as the radial displacement. Note that the eigen-function is shown as $r\xi_r$, allowing the 2D effect to be understood, thus, the mode expands in the poloidal direction. From the calculated eigen-function, it is predicted that the driving at the $q = 2$ surface is dominant. In such a high- β_N plasma, both $\nabla p(r)$ and $j(r)$ determine the MHD stability. The internal components $m = 1, 2, 3$ are driven by $\nabla p(r)$ and the external components $m \geq 4$ are driven by $j(r)$. Since the overall structure is localized at the low field side (LFS), this mode can induce an eddy current at the outer wall, suggesting that the stabilizing effect of the outer wall is larger than the inner one. At the moment, it is thought that the estimated eigen-function qualitatively agrees with that of the resistive wall, except near the wall region, and although the analysis does not take into account wall resistivity.

2.6 Plasma rotation profiles

In this experiment the RWM was observed as the plasma rotation was being reduced while keeping β_N constant by the stored energy feedback control. This means that the plasma rotation is considered to be capable of changing the stability of RWM from stable to unstable. Figure 8 gives the time evolution of the plasma rotation profiles measured using CXRS and with the q -profile measured using motional stark effect (MSE) spectroscopy [21]. After switching from counter-NB to co-NB the rotation profiles decelerated around the $q = 2$ surface. In particular, since the eigen-function estimated using MARG2D has a dominant component for $m = 2$ compared with the other poloidal components, the plasma rotation at $q = 2$ surface was thought to be effective in the stabilizing of the RWM. At the RWM onset the plasma rotation at $q = 2$ was around 0.5 kHz. This plasma rotation is considered to be the critical plasma rotation for RWM stabilization.

2.7 C_β vs plasma rotation diagram

It is found that the critical plasma rotation for RWM stabilization is much less than 1% of the Alfvén speed at the $q = 2$ surface. To clarify the dependence of the critical rotation on β_N , the target value used in the stored energy feedback control was systematically changed from shot to shot. Figure 9 provides the results obtained from the β_N -target scan as a C_β versus f_ϕ diagram, where C_β is defined as $C_\beta = (\beta_N - \beta_N^{\text{free}})/(\beta_N^{\text{ideal}} - \beta_N^{\text{free}})$. Namely $C_\beta = 0$ and 1 correspond to the no-wall ($\beta_N = \beta_N^{\text{free}}$) and ideal-wall ($\beta_N = \beta_N^{\text{ideal}}$) limits, respectively. The axes give the plasma rotation frequency f_ϕ and its corresponding nor-

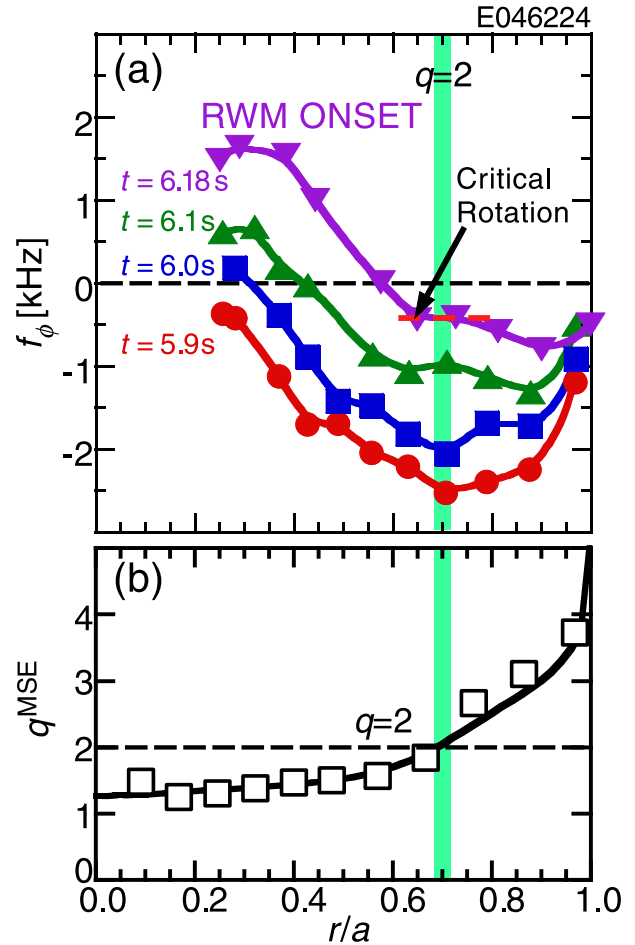


Fig. 8 (a) Time evolution of plasma rotation profiles after switching counter- to co-TANG-NBs until RWM onset and (b) q -profile at $t = 6.2$ s.

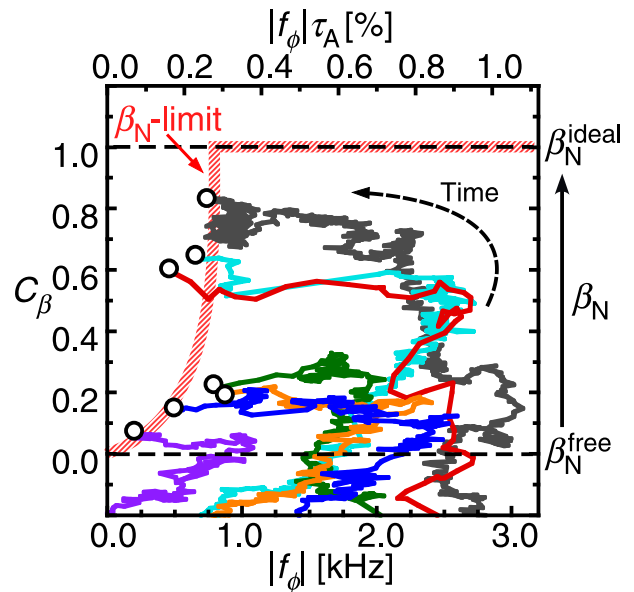


Fig. 9 Dependence of critical plasma rotation with RWM stabilization on C_β . Circles indicate the RWM onsets. The axes plot plasma rotation frequency f_ϕ and that normalized using the Alfvén time $f_\phi \tau_A$ at the $q = 2$ surface. The red curve corresponds to the discharge in Fig. 3.

malized value over the Alfvén time τ_A defined as $2\pi R/V_A$, where R and V_A are the major radius and the Alfvén speed, respectively.

Each trajectory corresponds to the time evolution of a single discharge, with the open circles revealing the onset of the RWM. In these discharges the plasma rotation was first accelerated in order to raise β_N . When β_N reached the target value of β_N the plasma rotation was reduced by switching the TANG-NBs as mentioned above. The RWMs were triggered when the plasma rotation became the critical value. The boundary in the diagram reveals the dependence of the critical rotation. The dependence on C_β is not strong, indicating that accessing β_N^{ideal} could be possible even with the slow plasma rotation $\sim 0.3\%$ of V_A . The results indicate that high- β_N operation up to β_N^{ideal} will be possible in ITER and a fusion reactor where the plasma rotation is predicted to be slower than 1% of the Alfvén speed.

3. Summary

We have carried out the experiments in order to investigate the rotational stabilization of the RWM in the JT-60U tokamak. The plasma rotation was controlled using a combination of TANG-NBs while keeping β_N constant using the stored energy feedback control. During the β_N constant phase the plasma rotation was only decelerated, and then an instability whose growth time was about 10 ms appeared. The slow growth time was equivalent to the resistive wall time of JT-60U. Compared with the instability observed in a high- β_p plasma with $d/a \simeq 1.7$ the growth time in a high- β_N plasma with $d/a \simeq 1.2$ was clearly slower. MARG2D analysis revealed that the achieved- β_N where the instability was observed would exceed β_N^{free} . From these results, the instability is identified as the RWM. Detailed measurement of the mode structure revealed that the RWM to have a clear $n = 1$ toroidal mode structure. Meanwhile, the poloidal mode structure was non-uniform, and thus the amplitude at the LFS was much larger than that at HFS. Namely, the RWM has a ballooning structure poloidally. This point completely differs from that of an instability such as the tearing mode, which only has a single poloidal component. The T_i -profiles measured using CXRS during the growth of the RWM reveal that the RWM to have a radially global mode structure. In addition, the RWM was slowly rotating with about τ_w^{-1} . The direction of the mode rotation was found to follow the direction of the plasma rotation at the $q = 2$ surface, which is also consistent with the MARG2D analysis and theoretical predictions. At the onset of the RWM the plasma rotation

at the $q = 2$ surface was less than 1 kHz, corresponding to about 0.3% of the Alfvén speed. Moreover, the dependence of the critical rotation on β_N was investigated by changing the target value of the stored energy feedback control. This resulted in the obtained dependence not being strong against C_β , which then means that a high- β_N operation up to β_N^{ideal} is possible in ITER and fusion reactors where a fast rotation can no longer be expected. It should be noted that experimental results obtained on DIII-D also suggest the slow critical rotation for the RWM stabilization [22–24]. On DIII-D high- β_N experiments took place by using balanced-NB injections based on a co-plasma rotation. Theoretically the kinetic effect would be considered to play an important role in a slow critical rotation [25, 26]. Based on the experimental results, the further research on the rotational stabilization of the RWM is required from both the theoretical and experimental points of view.

Acknowledgments

This work was supported in part by a Grant-in-Aid for Young Scientists (B) from the Ministry of Education, Culture, Sports, Science and Technology of Japan, No. 17760672 and No. 21760702.

- [1] ITER Physics Basis, Nucl. Fusion **47**, S285 (2007).
- [2] D. Pfirsch and H. Tasso, Nucl. Fusion **11**, 256 (1971).
- [3] A. Bondeson and D.J. Ward, Phys. Rev. Lett. **72**, 2709 (1994).
- [4] M.S. Chu *et al.*, Phys. Plasmas **2**, 2236 (1995).
- [5] M.S. Chu *et al.*, Phys. Plasmas **11**, 2497 (2004).
- [6] R. Fitzpatrick and A. Aydemir, Nucl. Fusion **36**, 11 (1996).
- [7] R. Fitzpatrick, Phys. Plasmas **9**, 3459 (2002).
- [8] ITER Physics Basis, Nucl. Fusion **39**, 2175 (1999).
- [9] S. Takeji *et al.*, J. Plasma Fusion Res. **78**, 447 (2002).
- [10] G. Matsunaga *et al.*, Plasma Phys. Control. Fusion **49**, 95 (2007).
- [11] G. Matsunaga *et al.*, Proc. 33rd EPS Conference on Plasma Physics (Roma, Italy), O2.003 (2006).
- [12] M. Takechi *et al.*, Phys. Rev. Lett. **98**, 055002 (2007).
- [13] M. Kuriyama *et al.*, Fusion Sci. Technol. **42**, 410 (2002).
- [14] M. Kuriyama *et al.*, Fusion Sci. Technol. **42**, 424 (2002).
- [15] K. Shinohara *et al.*, Plasma Fusion Res. **1**, 007 (2006).
- [16] N. Hosogane *et al.*, Fusion Sci. Technol. **42**, 368 (2002).
- [17] Y. Koide *et al.*, Rev. Sci. Instrum. **72**, 119 (2001).
- [18] S. Tokuda and T. Watanabe, Phys. Plasmas **6**, 3012 (1999).
- [19] W. Howl *et al.*, Phys. Fluid B **4**, 1724 (1992).
- [20] S. Takeji *et al.*, Fusion Sci. Technol. **42**, 278 (2002).
- [21] T. Fujita *et al.*, Fusion Eng. Des. **34-35**, 289 (1997).
- [22] H. Reimerdes *et al.*, Phys. Rev. Lett. **98**, 055001 (2007).
- [23] A.M. Garofalo *et al.*, Nucl. Fusion **47**, 1121 (2007).
- [24] E.J. Strait *et al.*, Phys. Plasmas **14**, 056101 (2007).
- [25] B. Hu and R. Betti, Phys. Rev. Lett. **93**, 105002 (2004).
- [26] Y. Liu *et al.*, Phys. Plasmas **15**, 092505 (2008).